Solar-Terrestrial Physics. 2019. Vol. 5. Iss. 2. P. 50–57. DOI: 10.12737/stp-52201908. © 2019 Jun Cheng, Yihua Yan, Dong Zhao, Long Xu. Published by INFRA-M Academic Publishing House
Original version: Jun Cheng, Yihua Yan, Dong Zhao, Long Xu, published in Solnechno-zemnaya fizika. 2019. Vol. 5. Iss. 2. P. 55–62. DOI: 10.12737/szf-52201908. © 2019 INFRA-M Academic Publishing House (Nauchno-Izdatelskii Tsentr INFRA-M)

SCALE SEQUENTIALLY CLEAN FOR MINGANTU SPECTRAL RADIOHELIOGRAPH

Jun Cheng
Key Laboratory of Solar Activity, National Astronomical Observatories, Chinese Academy of Sciences, Beijing, China, chengjun@nao.cas.cn
State Key Laboratory of Space Weather, Chinese Academy of Sciences, Beijing, China, chengjun@nao.cas.cn

Yihua Yan
Key Laboratory of Solar Activity, National Astronomical Observatories, Chinese Academy of Sciences, Beijing, China, yyh@nao.cas.cn

Dong Zhao
Key Laboratory of Solar Activity, National Astronomical Observatories, Chinese Academy of Sciences, Beijing, China, dzhao@nao.cas.cn

Long Xu
Key Laboratory of Solar Activity, National Astronomical Observatories, Chinese Academy of Sciences, Beijing, China, lxu@nao.cas.cn

Abstract. MingantU SpEctral Radioheliograph (MUSER) is a solar-dedicated radio heliograph, adopting aperture synthesis technique to image the Sun in the frequency range of 0.4 GHz to 15 GHz. MUSER has extremely high spatial resolution, temporal resolution, and frequency resolution beyond those of contemporary devices of the same category. For aperture synthesis, the number of antennas is limited, so sparse sampling of Fourier components is actually obtained for solar observation, which corresponds to the situation that a clean image is convolved by a dirty beam with strong sidelobe in a spatial domain. Thus, the deconvolution, such as CLEAN, is generally required for imaging the aperture synthesis to remove artifacts caused by the convolving dirty beam. The traditional Högbom CLEAN is based on the assumption that an observed object is only composed of point sources. This assumption does not hold for solar observation, where the solar disk is an extended source containing complex structures and diffuse features. In this paper, we make the first attempt to employ scale sequentially CLEAN for MUSER imaging, including Multi-Resolution CLEAN and Wavelet CLEAN. The experimental results demonstrate that the scale sequentially CLEAN, especially wavelet CLEAN, is superior to the traditional CLEAN algorithm in smaller number of iterations and improved image quality. We provide optimized wavelet parameters to further improve the performance of wavelet CLEAN.

Keywords: MUSER, Multi-Resolution CLEAN, Wavelet CLEAN, solar image.

INTRODUCTION

Solar radio observation provides important information about solar activity from the ground and allows us to diagnose solar activity parameters such as magnetic field, electron density, plasma temperature, etc. [Perley et al., 1989]. In order to build a solar radio telescope with high angular resolution, it would be necessary to build antenna with larger diameter, but this is sometimes unrealistic. Alternatively, to use an aperture synthesis telescope, which consists of a group of small antennas to image the Sun, and the resolution is proportional to the farthest distance between the extremities of the antennas [Koshiishi et al, 1994]. There are four famous solar-dedicated aperture synthesis radio heliographs put into use in the world: Japan's Nobeyama Radioheliograph (NORH) [Nakajima et al., 1995], France's Nancay Radio Heliograph (NRH) [Kerdraon, Delouis, 1997], Russia's Siberian Radio Heliograph (SRH) [Grechnev et al., 2018], and China's MUSER [Yan et al., 2009]. While the available frequencies are only 17 and 34 GHz in NORH [Nakajima et al., 1995], and five discrete frequencies in the range 150–450 MHz in NRH [Kerdraon, Delouis, 1997], and 26 discrete frequencies in the range 4000–8000 MHz in SRH, there are multiple frequencies in the range 0.40–15.00 GHz (64 for MUSER-I and 528 for MUSER-II) in MUSER. Moreover, MUSER has a capability of imaging the Sun every 3 ms and producing 3–5 TB data every day. This poses a huge challenge for rapid imaging processing.

According to the principle of synthetic aperture imaging, the visibilities collected by radio interferometers, composed of two antennas each, can be converted into a brightness, i.e., a spatial image of the sky object through inverse Fourier transform [Kochanov et al., 2013]. In general, the nonlinear deconvolution is required to remove artifacts in interferometric maps, which suffer from incomplete sampled visibility data in the Fourier (or called UV) domain: missing baselines; missing or deleted hour-angle ranges; unmeasured short-baseline information. The CLEAN algorithm is one of the most successful deconvolution algorithms used in radio astronomy for image restoration. The first CLEAN algorithm, which was devised by J. Högbom [1974], is based on the assumption that the object (the real image) is composed only of point sources [Starck, et al. 2002]. A simple iterative approach is used to find the point with the largest absolute brightness and to subtract PSF (dirty beam) scaled with the intensity at the point and loop gain. The final deconvolved image, known as the CLEAN image, is the sum of these point components convolved with a CLEAN beam, usually Gaussian,

with the resulting residual image added. Limitations of this algorithm such as excessive computational time and its failure to restore diffuse features have been discussed many times; and several algorithms have been invented with the aim of correcting some deficiencies of CLEAN. Clark [1980] proposed an improved CLEAN algorithm based on FFT, which had two cycles: major and minor [Napier et al., 1983]. Cotton-Schwab improved the Clark algorithm, which was often faster than before [Schwab, et al., 1984; Torrence et al., 1998]. Steer et al. [1984] proposed another improved Clark algorithm [Carilli et al., 1999]. Keel [1988] proposed the δ-CLEAN algorithm, where instead of searching for the maximum in dirty image residuals, one searched for the peak in the signal-to-noise ratio at each pixel. Koshiishi [2003] reported that the time required to process the Nobeyama solar image by the Steer algorithm was only 1/10 of the Högbom algorithm [Koshiishi, 2003]. Bethi presented that the basic CLEAN procedure was performed in two steps in each dimension to improve the calculation speed for Brazilian Decametric Array [Bethi et al., 2004]. However, until the scale-sensitive CLEAN algorithms appeared, all the above ones were scale-less CLEAN algorithms, which worked well only on isolated sources and failed on extended and complex objects, which were not composed only of point sources, but of sources of many different sizes and scales.

There are two kinds of scale-sensitive algorithms: scale sequentially CLEAN and scale simultaneously CLEAN respectively. As for the scale sequentially CLEAN, one of the first such methods, Multi-resolution CLEAN (MRC) proposed by Wakker end Schwarz [1988], tackles the problem by smoothing and decimating a dirty image and PSF to emphasize the extended emission. And then the standard CLEAN algorithm processes them separately to reconstruct the two clean maps at full resolution. To improve the scale number, Starck proposed the Wavelet CLEAN after MRC [Starck et al., 1994, 2002; Bhatnagar et al., 2004]. The Wavelet CLEAN uses the wavelet transform in the CLEAN process, which basically operates in a similar manner to MRC. In [Horiuchi, 2001], S. Horiuchi compared deconvolution results using CLEAN and the Wavelet CLEAN to simulate data, but this Wavelet CLEAN was very special — it just convolved a dirty map with a dirty beam to overcome the subjectivity in setting CLEAN boxes. In 2017 [Cheng et al., 2017a], we implemented the normal concept of the Wavelet CLEAN algorithm proposed by Starck. The preliminary simulation results show that the Wavelet CLEAN algorithm is superior to the Högbom CLEAN in the higher peak signal-to-noise ratio (PSNR) and lower root-mean-square error (RMSE). As for the scale simultaneously CLEAN, instead of working on each scale sequentially like the above scale sequentially CLEAN, it works simultaneously on all the scales considered, for example the Multi-Scale CLEAN proposed by Cornwell [2008] works in this way [Cornwell, 2008; Dong et al., 2017]. In this paper, we focus on the scale sequentially CLEAN due to the following reasons. (1) For MUSER's extensive data, the processing speed is important. The Multi-Scale CLEAN is more time consuming. (2) in wavelet, the signal-to-noise ratio of these coefficients is high, which may result in a higher CLEAN speed since it is much easier to find the pix.

The rest of this paper is organized as follows: Section II presents the image pipeline of MUSER. Section III provides experimental results on the scale sequentially CLEAN. The conclusions are given in the last section.

1. PIPELINE OF MUSER IMAGING

MUSER is an aperture synthesis radio heliograph situated in Inner Mongolia of China (latitude 42°12′42.6″ N, longitude 115°15′1.8″ E, altitude 1365 m), which has the capability to image the Sun at multiple frequencies (0.40–15.00GHz) with high time resolution, high spatial resolution, and high frequency resolution [Cheng et al., 2017b]. There are two arrays of 100 antennas arranged in three spiral arms: the high frequency array (MUSER-II) and the low frequency array (MUSER-I). The detailed parameters and antenna distribution of MUSER are given in Table 1 and Figure 1 separately.

The pipeline of MUSER image processing was constructed by MUSER's research group in 2016 (Figure 2). There are three main steps: pre-processing, dirty image processing, and clean image processing.

1.1. Multi-Resolution CLEAN

The Multi-Resolution CLEAN has developed a simple strategy for running the CLEAN algorithm to emphasize a broad emission first and then a finer resolution. The MRC approach converts both the dirty image and dirty beam into two intermediate images: the first one (called smooth map) by smoothing the data to a lower resolution with Gaussian, and the second one (called difference map) by subtracting the smoothed images from the original data. These two images are then treated separately. By using the standard CLEAN for them, the smoothed clean map and difference clean map are obtained. The recombination of these two maps give the clean map at full resolution. We can see two scales in MRC. The framework is shown in Figure 3.

As for the basic CLEAN process, firstly we get the ideal beam B^{I} through the Gauss fitting of the dirty beam B^{D}, then the key aspect is that it iteratively solves for positions and strengths of the CLEAN components in the residual image I^{R} and begins from I^{D}, which is defined as follows,

$$I^{\mathrm{C}}(i) = \sum_{(q=1)}^{i} I^{\mathrm{R}}_{(\max,q)} \sigma(x - x_q)\sigma(y - y_q). \quad (1)$$

Where i is the current iteration; $I^{\mathrm{R}}_{(\max,q)}$ and (x_q, y_q) are the value and position of the global peak point in the residual image I^{R} respectively.

$$I^{\mathrm{R}}(i) = I^{\mathrm{D}} - B^{\mathrm{D}} \cdot Gain \cdot I^{\mathrm{C}}(i-1). \quad (2)$$

On finding the i component, the residual image is simply updated by subtracting a suitably scaled and centered copy of PSF. Then, we repeat the process until the threshold is reached.

Table 1

Technical specifications of MUSER [Nakajima et al., 1995]

Parameters	MUSER-I	MUSER-II
Frequency range, GHz	0.4–2.0	2.0–15
Antenna Number	40	60
Antenna size, m	4.5	2
The maximum baseline, m	~3000	~3000
The minimum baseline, m	~8	~4
Frequency channels	64	528
Time resolution, ms	25	206.25
Spatial resolution	51.6″–10.3″	10.3″–1.4″
Image dynamic range, dB	≥25	≥25
Polarization	left, right	left, right

Figure 1. MUSER

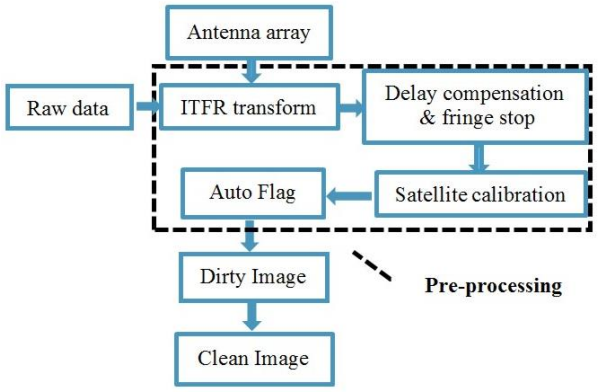

Figure 2. Imaging pipeline of MUSER

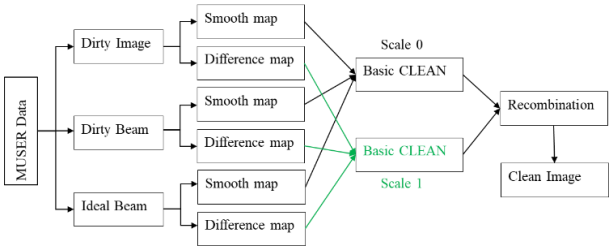

Figure 3. Framework of the Multi-Resolution CLEAN

1.2. Wavelet CLEAN

The Wavelet CLEAN means that we apply the basic CLEAN to each plane of the wavelet transform. The wavelet transform is widely used in the field of image processing with its excellent time domain, frequency domain localization capability, direction selection capability, and multi-resolution analysis capability consistent with the characteristics of human eyes. Nowadays, we can easily use the wavelet tool to achieve multiresolution, which does not impede the use of this algorithm. The important thing is that we can set more than two scales. The 2D wavelet decomposition using three resolution levels is shown in Figure 4.

$$DWT(j,k_1,k_2) = \\ = 2^j \sum^{l_1} \sum^{l_2} f(l_1,l_2)\varphi(2^j l_1 - k_1, 2^j l_2 - k_2). \quad (3)$$

The 2D wavelet transform firstly decomposes an image into three wavelet coefficient bands (horizontal, vertical, and diagonal) and one smoothed array. The same process on scale j is then repeated at the smoothed array on scale j+1, as shown in Equation 3. The wavelet CLEAN method here includes applying the 2D wavelet decomposition to both a dirty image and a dirty beam. To each scale, we apply the basic CLEAN algorithm and then use the 2-D wavelet reconstruction to get the final clean image. The framework is shown in Figure 5.

2. EXPERIMENTAL RESULTS AND DISCUSSION

We have first operated the Multi-Resolution CLEAN and Wavelet CLEAN for a simulated image to test the suitability of the solar source, and compared them to select the appropriate parameters. In order to objectively evaluate and compare image quality, we applied the peak signal-to-noise ratio (PSNR) and structural similarity index (SSIM) between clean images and ideal images, and the root-mean-square error (RMSE) in two residual images in successive iterations. PSNR and SSIM

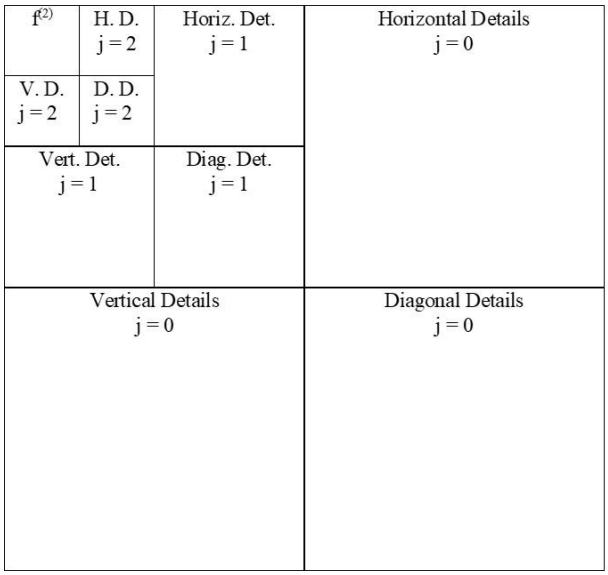

Figure 4. 2D wavelet decomposition using three scales

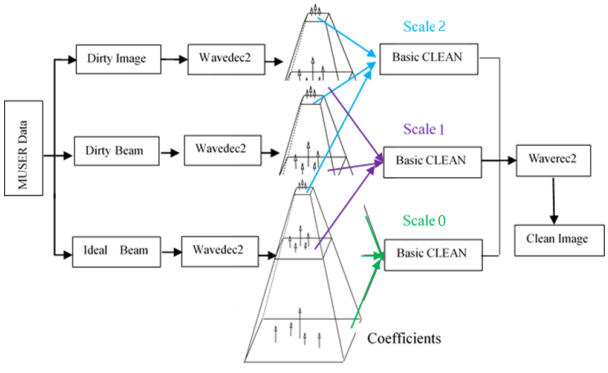

Figure 5. Framework of the Wavelet CLEAN

can reflect the similarity between restored images and ideal images, so the higher the better. RMSE can evaluate the efficiency of the CLEAN algorithms, the lower the better. Then, we applied the Multi-Resolution CLEAN and Wavelet CLEAN to a real MUSER image.

2.1. Evaluations and discussions of simulated image

In our simulation, an image with the size of 1024×1024 taken by the Atmospheric Imaging Assembly (AIA) from the Solar Dynamics Observatory (SDO) on November 1, 2015 was used as an ideal image and was convolved by the dirty beam obtained from MUSER-I on the same day to capture the simulated dirty image (Figure 6).

2.1.1. Discussion on the Multi-Resolution CLEAN

It is worth mentioning that in MRC, a smooth ideal image was taken by a Gaussian low-pass filter, and the FWHM (Full Width Half Maximum) ratio between the original and smoothed dirty beams was two. Figure 7 shows the smoothed and difference maps of the simulated dirty image, as well as restored images of MRC and Högbom CLEAN. There is an excessive false source in the Högbom CLEAN. From Table 2, we can easily find that the MRC image is better than the Högbom CLEAN image, with higher PSNR and SSIM and lower RMSE.

2.1.2. Discussion on the Wavelet CLEAN

Unlike the standard Fourier transform, the wavelet function used in the wavelet analysis is not unique, i.e. there are many available wavelet names (wname):

- Daubechies: db1, db2, ..., db45;
- Coiflets: coif1, ..., coif5;
- Symlets: sym2, ..., sym8, ..., sym45;
- Discrete Meyer wavelet: dmey.

Table 2

Comparison between simulated images

Parameters	Högbom CLEAN	MRC
PSNR	10.0051	12.5941
RMSE	0.0013	0.0012
SSIM	0.2514	0.2567

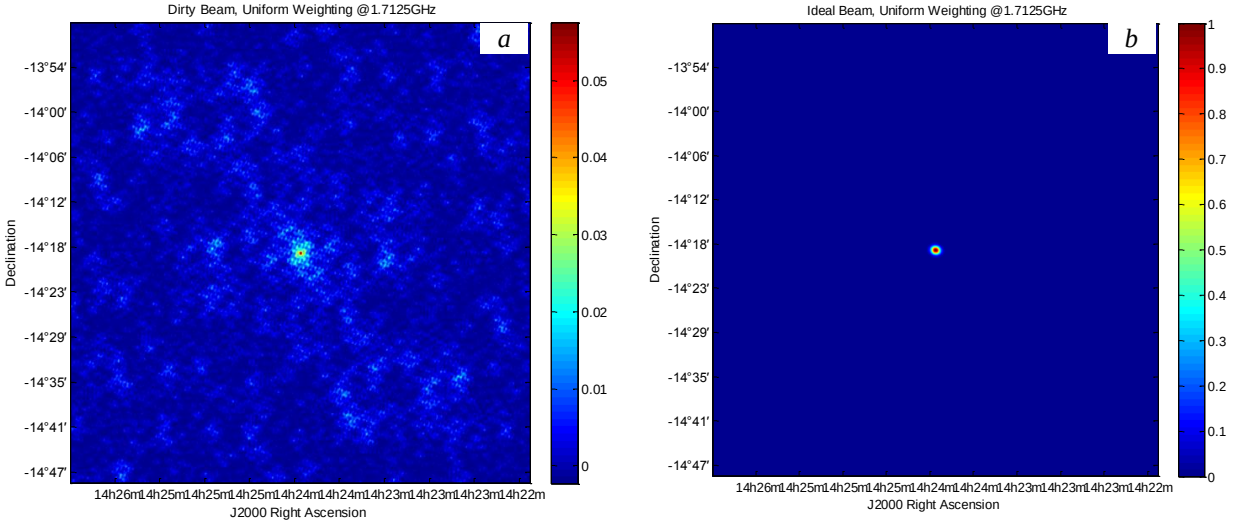

Figure 6. Simulated image on November 1, 2015: dirty beam from MUSER (*a*); clean beam from MUSER (*b*); AIA304 image (simulated ideal image) (*c*); simulated dirty image (*d*)

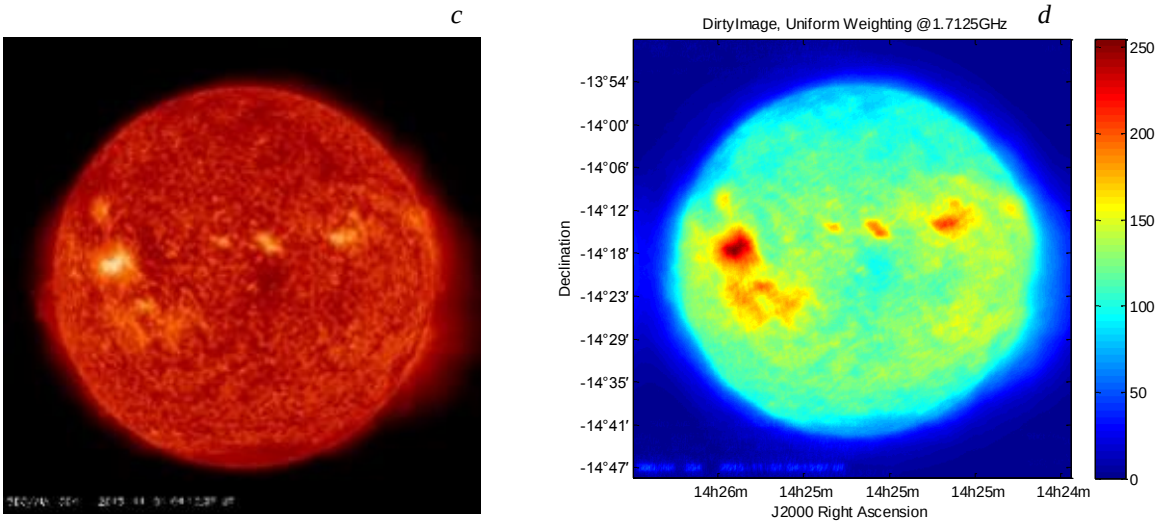

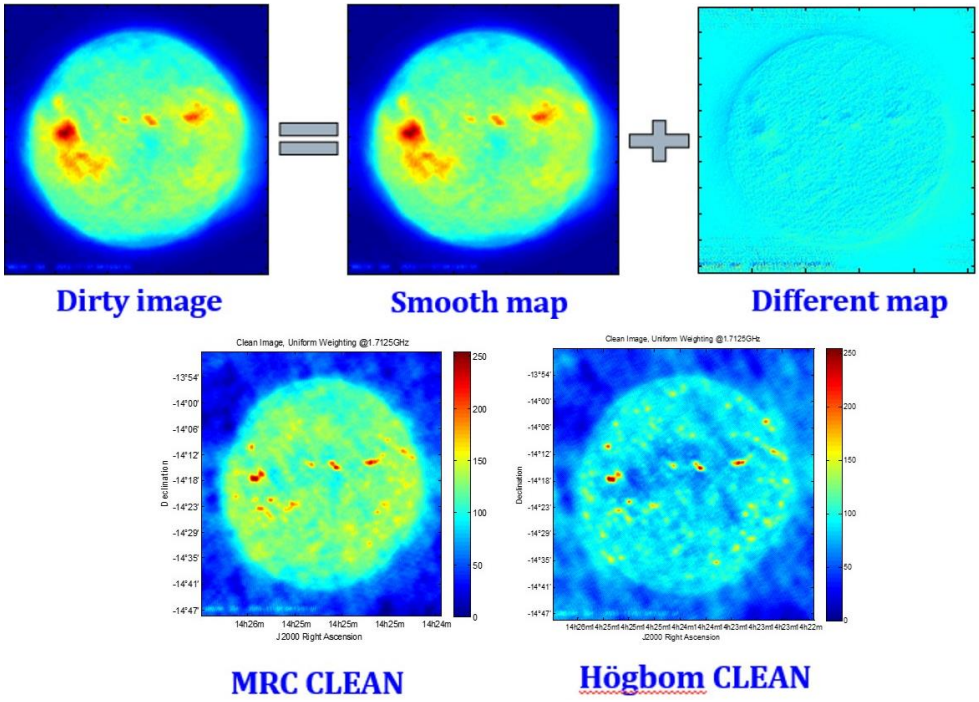

Figure 7. Simulated dirty image and restored images from MRC and Högbom CLEAN

For the same simulated dirty image, the different wavelet basis functions used in the Wavelet CLEAN provide different clean images. Another factor that is not unique is the wavelet scale, which also gives different clean images. From [Cheng et al., 2017a], we have found found that the scale number of wavelet decomposition is not as large as possible. When the number of layers is smaller than the number of layers of the image itself, the level of the image cannot be separated smoothly, so the single-layer wavelet decomposition effect does not work well; when the decomposition layer is too high, noise information is mistaken for high-frequency information. Through many experiments, along with visual judgment and objective evaluation, we can draw the conclusion that the result of scale 3, db2 or sym2 wavelet basis is best to deal with the dirty image on this sample. The reason for the same result is that the filter parameters of db2 and sym2 are the same. Figure 8 shows a restored image based on the Wavelet and Högbom CLEAN.

For the same simulated dirty image, the different wavelet basis functions used in the Wavelet CLEAN provide different clean images. Another factor that is not unique is the wavelet scale, which also gives different clean images. From [Cheng et al., 2017a], we have found found that the scale number of wavelet decomposition is not as large as possible. When the number of layers is smaller than the number of layers of the image itself, the level of the image cannot be separated smoothly, so the single-layer wavelet decomposition effect does not work well; when the decomposition layer is too high, noise information is mistaken for high-frequency information. Through many experiments, along with visual judgment and objective evaluation, we can draw the conclusion that the result of scale 3, db2 or sym2 wavelet basis is best to deal with the dirty image on this sample. The reason for the same result is that the filter parameters of db2 and sym2 are the same. Figure 8 shows a restored image based on the Wavelet and Högbom CLEAN.

2.2. Evaluations and discussions on MUSER image

First, we obtained a dirty image of MUSER-I on November 1, 2015 from the imaging pipeline of MUSER. Then carried out the Högbom CLEAN and scale sequentially CLEAN separately on this dirty image. Figure 9 shows the best results of each method. It is worth to mention that the parameters of the Wavelet CLEAN used here are the same as those of the above best one of the simulated images. It is easy to find that the red part source area of the MRC image is larger than the Högbom CLEAN image, which means that MRC is better than the Högbom CLEAN for MUSER images, but

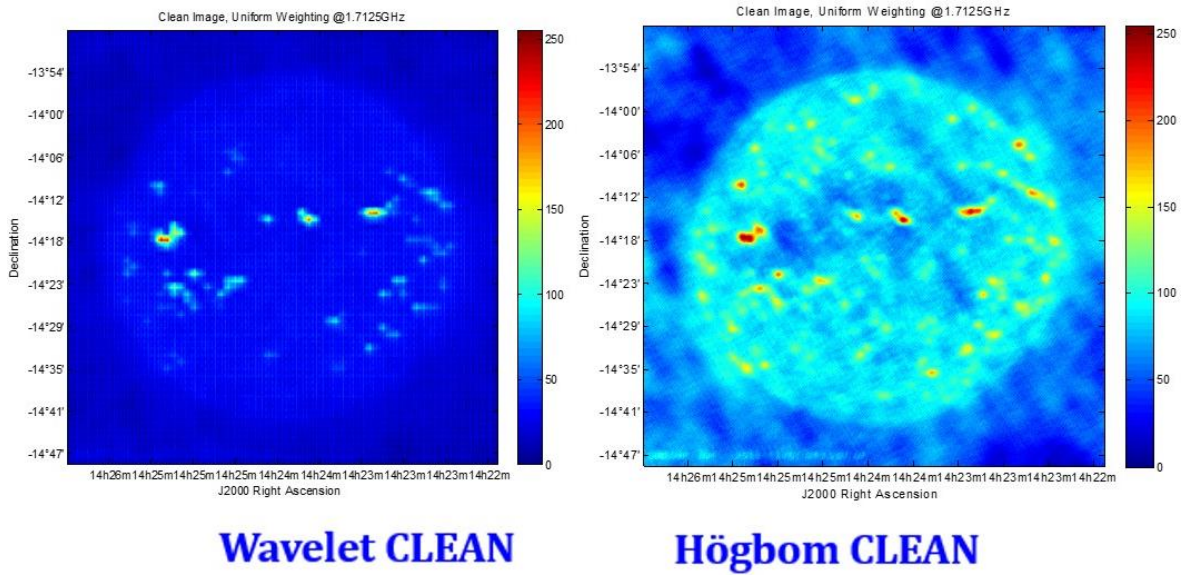

Figure 8. Wavelet and Högbom CLEAN restored images

Table 3

Comparison between simulated images

Parameters	Högbom CLEAN	Wavelet CLEAN	
PSNR	10.0051	db2	16.5726
RMSE	0.0013		0.0029
SSIM	0.2514		0.2132
PSNR		coif3	16.1785
RMSE			0.0043
SSIM			0.2527
PSNR		sym2	16.5726
RMSE			0.0029
SSIM			0.2132
PSNR		dmey	25.8288
RMSE			0.0132
SSIM			0.2132

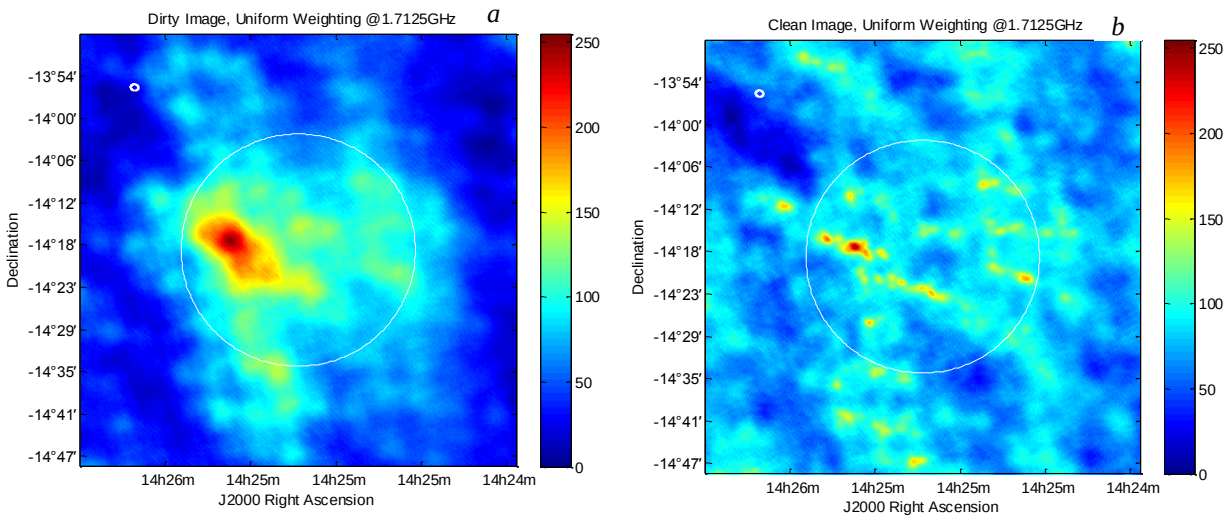

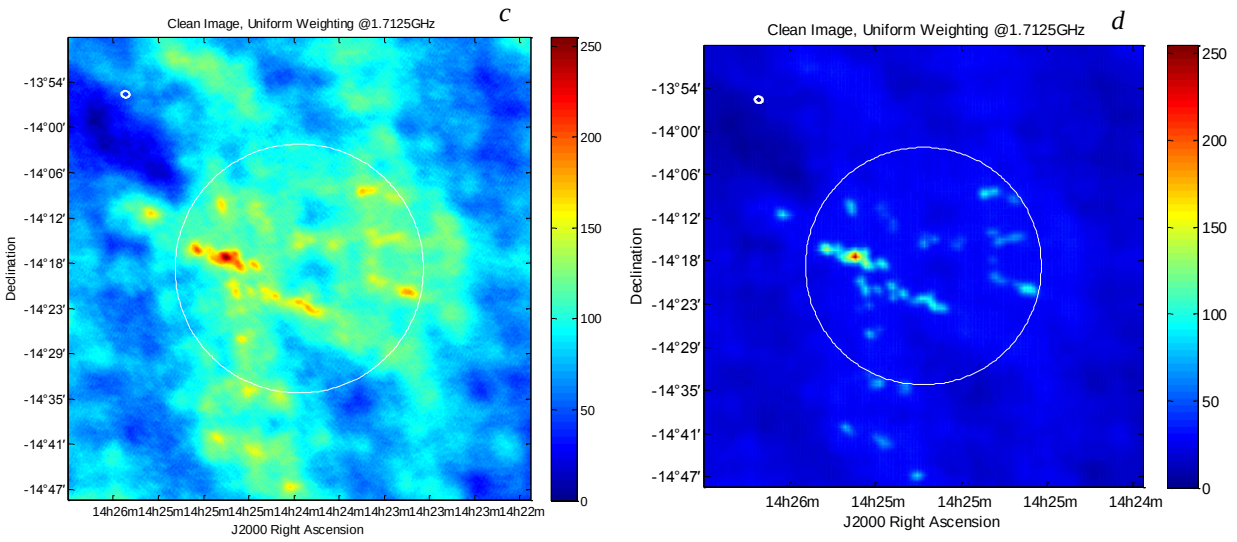

Figure 9. Real image: MUSER dirty image (*a*); Högbom CLEAN image (*b*); MRC image (*c*); Wavelet CLEAN image (*d*)

but there is some false information (red dot) both in the Högbom CLEAN image and the Multi-Resolution CLEAN image. The advantage of the Wavelet CLEAN is demonstrated at this point.

CONCLUSION

This paper presents the scale sequentially CLEAN, including the Multi-Resolution CLEAN and Wavelet CLEAN on both simulate and real dirty images from MUSER. We have demonstrated how the Wavelet CLEAN can be used to address some problems of the Högbom CLEAN for low signal-to-noise maps and for an extended source, especially for solar radio imaging. Furthermore, parameters of the Wavelet CLEAN have been optimized and discussed in experiments and comparisons.

This work was supported by the Specialized Research Fund for State Key Laboratories under Grant No. 2018-026F-04 and also by the National Natural Science Foundation of China under Grant Nos. 6171101371, 11773043, and 11793035.

REFERENCES

Bethi N.K., Preto A.J., Stephany S., Faria C., Rosa R.R., Sych R., Sawant H.S. An optimized implementation of the CLEAN method for the BDA. *Research Gate*. 2004. URL: https://www.researchgate.net/publication/268286641.

Bhatnagar S., Cornwell T.J. Scale sensitive deconvolution of interferometric images. Adaptive Scale Pixel (ASP) decomposition. *Astron. Astrophys*. 2004, vol. 426, pp. 747–754. DOI: 10.1051/0004-6361:20040354.

Carilli C.L., Taylor G.B., Perley R.A. Synthesis imaging in radio astronomy II. A Collection of Lectures from the Sixth NRAO/NMIMT Synthesis Imaging Summer School. *ASP Conf. Ser*. 1999, vol. 180.

Cheng J., Xu L., Yu X., Chen L., Wang W., Yan Y. Auto-flag the baseline for Mingantu Spectral Radioheliograph with LSTM. *IEEE Visual Communications and Image Processing (VCIP)*. St. Petersburg, FL, USA, 2017a. DOI: 10.1109/VCIP.2017.8305098.

Cheng J., Xu L., Lu Z., Zhao D. Application of Wavelet CLEAN for Mingantu Spectral Radioheliograph Imaging. *IEEE ISPACS*. Xiamen, China, 2017b. DOI: 10.1109/ISPACS.2017.8266450.

Clark B.G. An efficient implementation of the algorithm CLEAN. *Astronomy and Astrophysics*. 1980, vol. 89, no. 3, p. 377. DOI: 10.1007/BF00167710.

Cornwell T.J. Multiscale CLEAN deconvolution of radio synthesis images. *IEEE Journal of Selected Topics in Signal Processing*. 2008, vol. 2, iss. 5, pp. 793–801. DOI: 10.1109/JSTSP.2008.2006388.

Dong Z., Xu L., Cheng L.J., et al. Multi-Scale CLEAN deconvolution for solar radio imaging with Mingantu Spectral Radioheliograph (MUSER). *IEEE ISPACS*. Xiamen, China, 2017.

Grechnev V.V., Lesovoi S.V., Kochanov A.A., Uralov A.M., Altyntsev A.T., Gubin A.V., et al. Multi-instrument view on solar eruptive events observed with the Siberian Radioheliograph: From detection of small jets up to development of a shock wave and CME. *J. Atmos. Solar-Terr. Phys*. 2018. vol. 174, pp. 46–65. DOI: 10.1016/j.jastp.2018.04.014.

Högbom J.A. Aperture synthesis with a non-regular distribution of interferometer baselines. *Astronomy and Astrophysics Supplement Series*, 1974, vol. 15, p. 417.

Horiuchi S., Kameno S., Ohishi M. Developing a wavelet CLEAN algorithm for radio-interferometer imaging. *Astronomical Data Analysis Software and Systems X, ASP Conf. Ser*. 2001. vol. 238, p. 529.

Keel W.C. The optical continua of extragalactic radio jets. *Astrophys. J*. 1988, vol. 329, p. 532.

Kerdraon A., Delouis J.M. The Nancay Radioheliograph. *Coronal Physics from Radio and Space Observations: Proc. CESRA Workshop*. Nouan le Fuzelier, France, 3–7 June 1996. Springer Berlin Heidelberg. 1997, vol. 483, pp. 192–201. DOI: 10.1007/BFb0106458.

Kochanov A.A., Anfinogentov S.A., Prosovetsky D.V., Rudenko G.V., Grechnev V.V. Imaging of the solar atmosphere by the Siberian Solar Radio Telescope at 5.7 GHz with an enhanced dynamic range. *Publications of the Astronomical Society of Japan*. 2013, vol. 65, pp. 2226–2237. DOI: 10.1093/pasj/65.sp1.S19.

Koshiishi H. Restoration of solar images by the Steer algorithm. *Astron. Astrophys*. 2003, vol. 412, pp. 893–896. DOI: 10.1051/0004-6361:20031514.

Koshiishi H., Enome S., Nakajima H., Shibasaki K., Nishio M., Takano T., et al. Evaluation of the imaging performance of the Nobeyama Radioheliograph. *Publications of the Astronomical Society of Japan*. 1994, vol. 46, pp. L33–L36.

Nakajima H., Nishio M., Enome S., Shibasaki K., Takano T., Hanaoka Y., et al. New Nobeyama Radio Heliograph. *J. Astrophys. Astron. Suppl*. 1995, vol. 16, pp. 437.

Napier P.J., Thompson A.R., Ekers R.D. The Very Large Array: design and performance of a modern synthesis radio telescope. *Proc. IEEE*. 1983, vol. 71, pp. 1295–1320.

Perley R.A., Schwab F.R., Bridle A.H. Synthesis imaging in radio astronomy: a collection of lectures from the third NRAO synthesis imaging summer school. *ASP Conf. Ser*. 1989, vol. 6.

Schwab F.R. Relaxing the isoplanatism assumption in self-calibration; applications to low-frequency radio interferometry. *The Astronomical Journal*. 1984, vol. 89, pp 1076–1081. DOI: 10.1086/113605.

Starck J.L., Murtagh F. Image restoration with noise suppression using the wavelet transform. *Astronomy and Astrophysicsю*. 1994, vol. 288,pp. 342–348.

Starck J.L., Pantin E., Murtagh F. Deconvolution in Astronomy: A Review. *Publications of the Astronomical Society of the Pacific*. 2002, vol. 114, pp. 1051–1069. DOI: 10.1086/342606.

Steer D.G., Dewdney P.E., Ito M.R. Enhancements to the deconvolution algorithm CLEAN. *Astronomy and Astrophysics*. 1984, vol. 137, pp. 159–165.

Torrence C., Compo G.P. A practical guide to wavelet analysis. *Bulletin of the American Meteorological Society*. 1998, vol. 79, iss. 1, pp. 61–78. DOI: 10.1175/1520-0477(1998)079%3C0061:APGTWA%3E2.0.CO;2.

Wakker B.P., Schwarz U.J. The Multi-Resolution CLEAN and its application to the short-spacing problem in interferometry. *Astron. Astrophys*. 1988, vol. 200, no. 1-2, pp. 312–322.

Yan Y.H., Zhang J., Wang W., Liu F., Chen Z., Ji G. The Chinese Spectral Radioheliograph–CSRH. Earth, Moon, and Planets, China, 2009, vol. 104, iss. 1-4, pp. 97–100. DOI: 10.1007/s11038-008-9254-y.

How to cite this article:

Jun Cheng, Yihua Yan, Dong Zhao, Long Xu. Scale sequentially CLEAN for Mingantu Spectral Radioheliograph. *Solar-Terrestrial Physics*. 2019. Vol. 5. Iss. 2. P. 50–57. DOI: 10.12737/stp-52201908.